VIP Concentric Patterns

DOI: 10.1002/ange.200804633

Robust Self-Assembly of Highly Ordered Complex Structures by Controlled Evaporation of Confined Microfluids**

*Suck Won Hong, Myunghwan Byun, and Zhiqun Lin**

The evaporative self-assembly of nonvolatile solutes such as polymers, nanocrystals, and carbon nanotubes has been widely recognized as a nonlithographic means of producing a diverse range of intriguing complex structures.[1–5] The spatial variation of evaporative flux and possible convection mean, however, that these non-equilibrium dissipative structures (e.g., coffee rings,[6] fingering patterns,[7] and polygonal network structures[8]) are often irregular and stochastically organized. Yet for many applications in microelectronics, data storage devices, and biotechnology, it is highly desirable to achieve surface patterns that have a well-controlled spatial arrangement. To date, only a few elegant studies have centered on the precise control of the evaporation process to produce ordered structures.[9–17] When compared with conventional lithographic techniques, surface patterning by controlled solvent evaporation is simple, cost-effective, and offers a lithography and external-field-free means of organizing nonvolatile materials into ordered microscopic structures over large surface areas. For example, it has been recently demonstrated that constraining a drop of solution in a restricted geometry formed by placing a sphere against a flat substrate results in controlled evaporation. Consequently, the repetitive pinning and depinning of the solution's contact line produces a lateral surface pattern that consists of hundreds of concentric, highly ordered "coffee rings", the gradients of which vary in width and height.[12,13,17]

The ability to engineer an evaporative self-assembly process that yields a wide range of complex, self-organizing structures over large areas other than strictly concentric rings[12,13,17] offers tremendous potential for applications in electronics, optoelectronics, and sensors. The formation of periodic assemblies of polymeric squares, triangular contour lines, and ellipses would be effectively mediated by controlled solvent evaporation that is precisely guided by the shape of the curved upper surface of a confined curve-on-flat geometry. Herein, we demonstrate a facile, robust, and one-step method of evaporating polymer solutions in curve-on-flat geometries to create versatile, highly regular microstructures in a precisely controlled environment, as well as offering a comprehensive study of the influence of different upper surfaces on complex structure formation by controlled evaporation. Our method further enhances current fabrication approaches to creating highly ordered structures in a simple and cost-effective manner, with the potential to be tailored for use in photonics,[18] electronics,[19,20] optoelectronics,[21] microfluidic devices,[22] nanotechnology,[23] and biotechnology.[24]

A linear conjugated polymer, poly(2-methoxy-5-(2-ethylhexyloxy)-1,4-phenylenevinylene) (MEH-PPV, molecular weight = 50–300 kg mol^{-1}) was used as the nonvolatile solute. The choice of system was motivated by its numerous potential applications in the areas of light-emitting diodes, solar cells, and biosensors.[21] A solution of MEH-PPV in toluene was prepared at a concentration of 0.05 mg mL^{-1}. The key to our approach is the use of a simple confined geometry consisting of a curved upper surface on a flat lower substrate (curve-on-flat geometry) that forms a microscopic gap in which the MEH-PPV toluene solution is loaded; this results in a capillary-held microfluid (a liquid capillary bridge, see Figure 1a, Figure 3a, and the Experimental Section). The three curved surfaces used in the study were a square pyramid (the area of the sides = 1.0 × 1.0 cm^2 and $H_{pyramid}$ (pyramid height) = 100 μm (Figure 1a)), a triangular-slice sphere (R, (the radius of curvature) = 1.65 cm; D, the diameter = 1.5 cm; the arm width at A, C, and D = 800 μm (Figure 3a)), and a chisel lens (D = 1.0 cm, H_{chisel} (the chisel height) = 100 μm (Figure S2a in the Supporting Information). The surfaces were made of aluminum, stainless steel, and fused silica, respectively. Unlike previous work in which evaporation occurred over the entire droplet surface,[4–6,8] evaporation of the solvent in this case was restricted to the edge of the capillary within the curve-on-flat geometry (Figure 1a and Figure 3a).

Figure 1a,b, illustrates the route to concentric square stripes formed by evaporation in the square-pyramid-on-flat geometry. The loss of toluene at the capillary edge by evaporation triggered pinning of the contact line (the "stick"), thereby forming the outermost MEH-PPV square. During deposition of the MEH-PPV, the evaporation of toluene caused the initial contact angle of the capillary edge to gradually decrease to a critical angle, at which the capillary force (the depinning force) became greater than the pinning force.[25] This led the contact line to jump, or "slip," to a new position, thus developing a new square (Figure 1b).[12,25,26] It is worth noting that the pyramid (the upper surface) provided a unique environment to guide the "stick–slip" motions of the contact line of the evaporating MEH-PPV microfluid, thereby forcing MEH-PPV to deposit in a manner that conformed to the square-shaped sides of the pyramid

[*] S. W. Hong, M. Byun, Prof. Z. Lin
Department of Materials Science and Engineering
Iowa State University
Ames, IA 50011 (USA)
Fax: (+1) 515-294-7202
E-mail: zqlin@iastate.edu

[**] We gratefully acknowledge support from the National Science Foundation (CAREER award CBET-0844084) and 3M.

Supporting information for this article is available on the WWW under http://dx.doi.org/10.1002/anie.200804633.

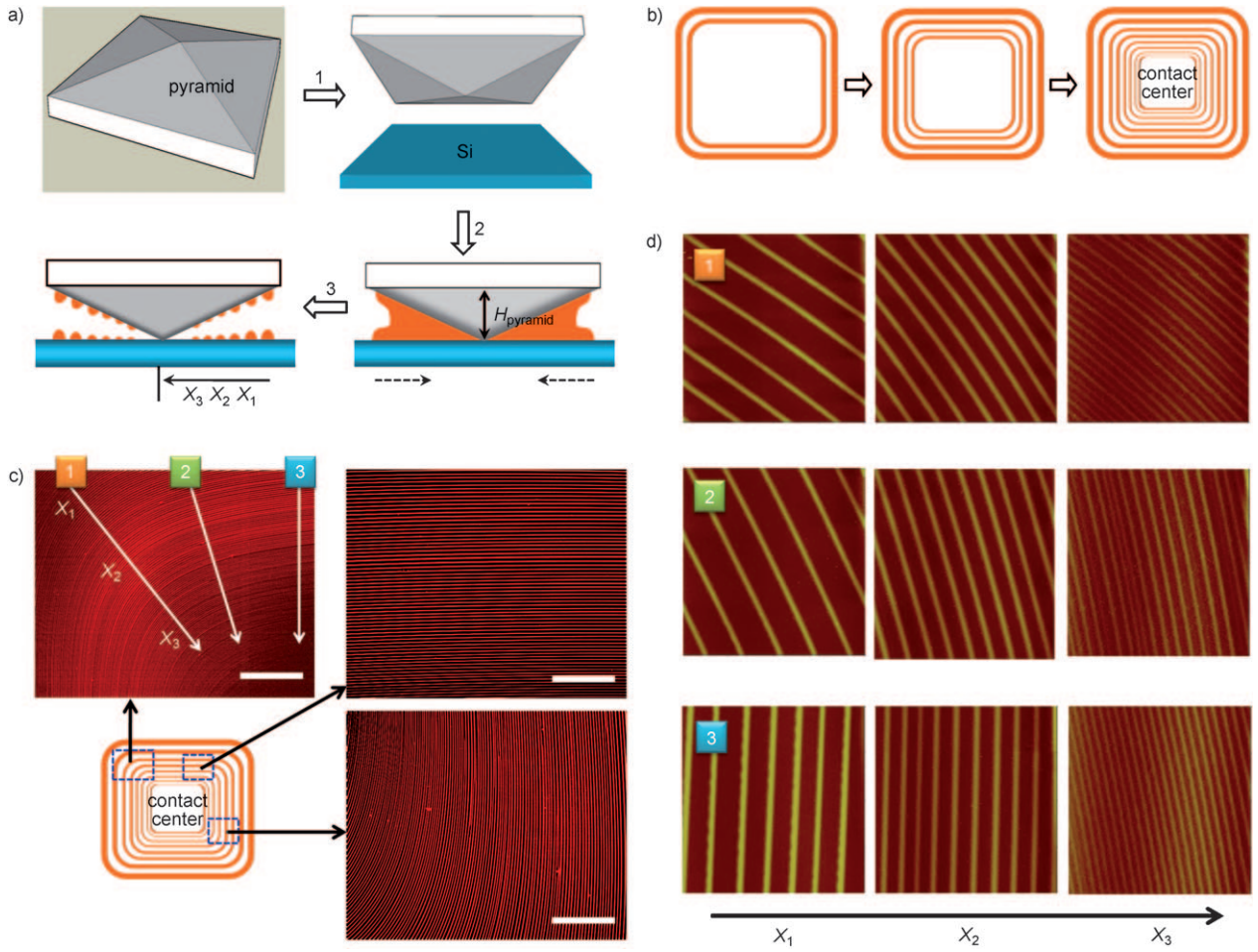

Figure 1. a) Schematic illustration of the route to gradient-concentric square stripes. A drop of MEH-PPV in toluene solution was trapped in a pyramid-on-flat geometry, which consisted of a square pyramid (upper left panel) situated on a Si substrate (upper right panel), by holding the solution in a capillary bridge (side view, lower right panel; the dashed arrows below the substrate denote movement of the solution front toward the center of the pyramid/Si contact; $H_{pyramid} = 100$ μm). As the solvent evaporated, gradient concentric square stripes of MEH-PPV were formed by successive controlled "stick–slip" motions of the contact line (side view, lower left panel). X_1, X_2, and X_3 are the distances of rings from the pyramid/Si contact center at the outermost region (X_1), the intermediate region (X_2), and the innermost region (X_3). b) Stepwise representation of the formation of gradient concentric square stripe propagating from the capillary edge toward the pyramid/Si contact center during solvent evaporation (top view). c) Representative fluorescence micrographs (top view) corresponding to locations defined in the lower left schematic (dashed blue boxes) show the bent stripes (upper left and lower right micrographs) and parallel straight stripes of MEH-PPV (upper right micrograph) formed on the Si substrate. Scale bars are 600 μm in the upper left and 300 μm in the upper and lower right images. d) AFM height images of surface patterns formed on the Si substrate taken along the directions marked by arrows 1, 2, and 3 in (c) as the "stick-slip" cycle progressively approached the pyramid/Si contact center, corresponding to the regions from X_1 to X_2 to X_3. Left column at X_1: MEH-PPV stripes with the largest $\lambda_{C\text{-}C}$ value were formed at the early stage of evaporation. Middle and right columns at X_2 and X_3, respectively: as the solution front moved inwards, $\lambda_{C\text{-}C}$ gradually decreased. The scanning area is 100 μm × 100 μm^2 for all images.

(Figure 1b). Consequently, repeated "stick–slip" cycles of the contact line resulted in the formation of hundreds of concentric squares of MEH-PPV (Figure 1c).

The evaporation in a typical experiment took less than half an hour to complete, leaving behind highly regular squares on both the pyramid and the Si substrate. Only surface patterns formed on the Si substrate were evaluated in the study. Because MEH-PPV allows fluorescence imaging, we were able to confirm that no MEH-PPV was deposited between the adjacent microscopic square stripes (Figure 1c). The fluorescence micrograph of concentric squares clearly shows a bend angle of 90° on the border of two facets of the square pyramid (upper left panel, Figure 1c), while parallel stripes were observed under the facets of the pyramid (upper right panel, Figure 1c). A transition from bent to parallel stripes is shown in the lower right panel of Figure 1c. These well-defined complex structures, which continued to the center of the pyramid/Si contact area over a surface up to one square centimeter depending on the dimensions of the pyramid used, reflect the synergy of the repeated "stick–slip" motion of the contact line and the order determined by the symmetry of the upper pyramid (Figure 1c).

Further scrutiny of the concentric patterns in Figure 1c by using atomic force microscopy (AFM) revealed that the squares were gradient rather than strictly repetitive. Representative AFM height images taken at different locations,

corresponding to the directions marked with arrows 1, 2, and 3 in the upper left micrograph of Figure 1c, are shown in Figure 1d. Efforts were made to ensure that the AFM imaging covered precisely the same squares at the three different locations. The center-to-center distance between adjacent squares, $\lambda_{C\text{-}C}$, decreased as the proximity to the pyramid/Si contact center increased (that is, from the outermost region X_1 to the innermost region X_3, where X is the distance from the pyramid/Si contact by taking the origin to be the center of the area labeled "contact center" (Figure 1a–c)), which can be attributed to competition between the linear pinning force and the nonlinear capillary force.[25] Figure 2 summarizes $\lambda_{C\text{-}C}$, width, w, and height, h, of the MEH-PPV stripes as a function of X. At location 1, as the evaporation front propagated toward the pyramid/Si contact center (from X_1 to X_3 in Figure 1c), the values of $\lambda_{C\text{-}C}$, w, and h decreased progressively, from $\lambda_{C\text{-}C} = 22.4$ μm, $w = 4.7$ μm, and $h = 22$ nm ($X_1 = 5700$ μm) to 11.9 μm, 4.2 μm, and 18 nm ($X_2 = 4400$ μm) and to 6.1 μm, 2.5 μm, and 12 nm ($X_3 = 3300$ μm; Figure 1d, first row). A similar trend for the values of $\lambda_{C\text{-}C}$, w, and h was observed at location 3, decreasing from $\lambda_{C\text{-}C} = 15.7$ μm, $w = 5.1$ μm, and $h = 27$ nm ($X_1 = 4800$ μm) to 5.8 μm, 2.3 μm, and 10 nm ($X_3 = 2400$ μm; Figure 1d, third row). Either on their own or as a part of squares (stripes in a parallel configuration, as in the upper right panel of Figure 1c), the square stripes can be considered as device-oriented structures, and may potentially be integrated into complex microelectronic, optical, optoelectronic, and sensing devices.

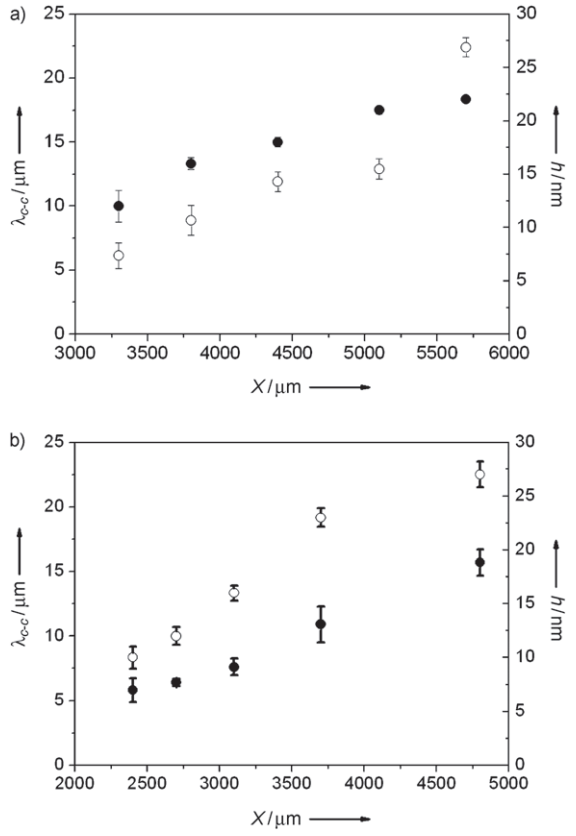

Figure 2. The center-to-center distance between the adjacent stripes, $\lambda_{C\text{-}C}$ (solid symbols), and the height of the stripes, h (open symbols), are plotted as a function of X, where X is the distance from the square pyramid/Si contact center along a) direction 1 and b) direction 3 in Figure 1c–d.

By replacing the square pyramid with a triangular-slice sphere as the upper component, a set of concentric triangular contour lines ("bent" lines) of MEH-PPV were produced. The construction of a triangular-slice-sphere-on-flat geometry is illustrated in Figure 3a. The intrinsic configuration of a triangular-slice sphere with three arms at A, C, and D (Figure 3a) guided the contact line of the receding MEH-PPV meniscus to "stick" and "slip" successively, thereby forming unique, regularly organized contour lines (Figure 3b). The fluorescence micrographs of hundreds of highly curved contour lines, which correspond to the blue-boxed regions defined in the schematic, are shown in Figure 3c.

Representative AFM height images taken along the directions denoted in Figure 3c (arrows 1, 2, and 3) are shown in Figure 3d. At location 1, gradient lines were formed by controlled "stick-slip" motions of the contact line of the MEH-PPV toluene solution that was confined directly between the arms of the triangular-slice sphere and the Si substrate (far left to far right in the first row of Figure 3d). Both $\lambda_{C\text{-}C}$ and h values decreased progressively, from $\lambda_{C\text{-}C} =$ 35.2 μm and $h = 44$ nm ($X_1 = 7100$ μm) to 10.9 μm and 16 nm ($X_2 = 4190$ μm) and to 4.3 μm and 5 nm at ($X_3 = 2800$ μm; Figure S1a in the Supporting Information). The number of lines in the 100×100 μm^2 scanning area increased from 3 lines (far left image) to 10 lines (third image) to 21 lines (far right image) in the first row of Figure 3d.

At location 3, the MEH-PPV line width first increased (third image in third row, Figure 3d) and then decreased continuously (fourth and fifth images). This may be because part of the MEH-PPV solution was not completely constrained between the body of the triangular-slice sphere (body B, Figure 3a) and the Si substrate. Instead, the solution extended outside the body of the triangular-slice sphere, thereby yielding an intriguing transition in the dimension of lines (third image) during solvent evaporation. This also partially explains the splitting of MEH-PPV into two thinner lines observed at location 2 (third and fourth images in the second row) because of the interference of the "stick" of the receding contact lines from directions 1 (thin lines) and 3 (thick lines). Nonetheless, data undulation along the X direction is clearly evident for $\lambda_{C\text{-}C}$ and h at location 3 (see Figure S1b in the Supporting Information). Branching at the transition region (location 2) can be attributed mainly to the difference in height between the MEH-PPV capillary bridge under the arm and the body of the triangular-slice sphere, where H_{body} is smaller than H_{arm} (Figure 3a), which led to a difference in the evaporation rate of the solvent. Because a larger capillary bridge has a higher evaporation rate,[27] the MEH-PPV meniscus beneath the arm retracted faster than that beneath the body of the triangular-slice sphere. The imbalance between the fast "stick–slip" cycles of the contact line caused by the larger capillary bridge (H_{arm}) and the slower "stick–slip" cycles at the smaller capillary entrance (H_{body}) was responsible for a locally branched pinning of the contact lines at location 2.[28] We note that such highly regular

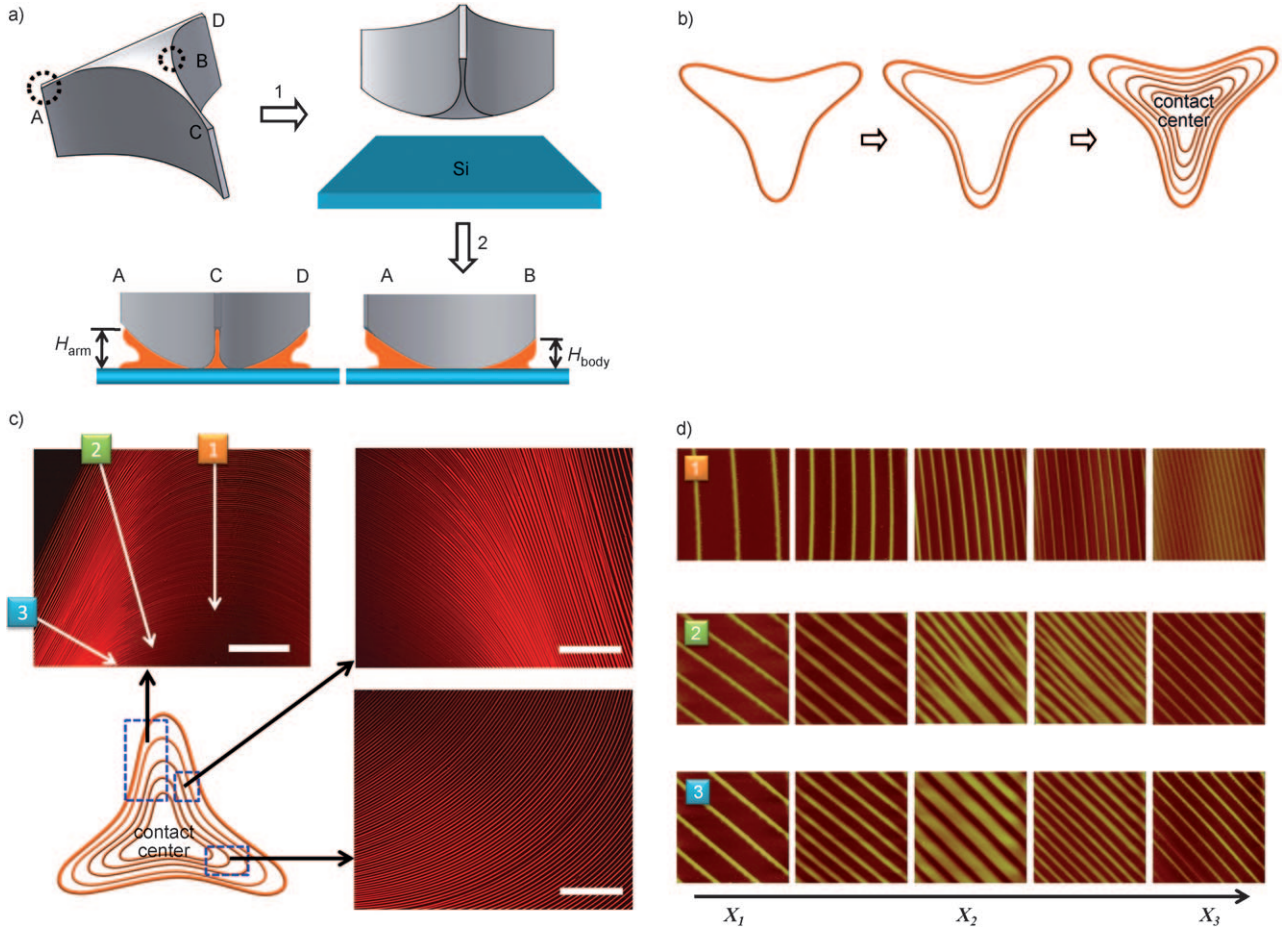

Figure 3. a) Schematic illustration of the construction of a triangular-slice-sphere-on-Si geometry in which a drop of MEH-PPV toluene solution was constrained, bridging the gap between the triangular-slice sphere and the Si substrate. The diameter of the sphere before being sliced triangularly was 1.5 cm, with a radius of curvature of 1.65 cm. The diameter of the central area in the triangular-slice sphere is 2 mm. The initial height of the capillary edges, H_{arm} and H_{body}, depended on the location of the trapped MEH-PPV solution. The H_{body} value under the body of the triangular-slice sphere was small, while the H_{arm} value under the arm was large (side view in lower panel). Left: looking at positions A and D from position C. Right: side view of positions A and B, where B is the midpoint of C, and D and is directly under the body. b) Stepwise representation of the formation of gradient concentric triangular contour lines in the triangular-slice-sphere-on-Si geometry. c) Representative fluorescence micrographs at different locations defined in the lower left schematic (dashed blue boxes) show the highly curved lines. The scale bars are 600 μm in the upper left and 300 μm in the upper and lower right images. d) AFM height images of surface patterns taken along the directions denoted by arrows 1, 2, and 3 in (c). Far left column at X_1: MEH-PPV stripes with the largest λ_{C-C} values were formed in the early stage of evaporation. Third column at X_2: as the solution front moved inwards, the λ_{C-C} value progressively decreased to the final stage (far right column at X_3). The branching of MEH-PPV into two thinner lines is evidenced in the third and fourth images at location 2 (middle row). The scanning area is 100 μm × 100 μm^2 for all images.

yet complex structures are difficult to fabricate by conventional means, but can be readily obtained using the present method.

A chisel lens was utilized to further demonstrate that the formation of such highly regular surface patterns can be dynamically tuned by the choice of the shape of the upper curved surface in confined geometries. The chisel lens was placed vertically with the border of its two facets in contact with the Si substrate, to form a chisel lens on flat geometry (Figure S2a in the Supporting Information). Hundreds of concentric ellipses were formed, which appeared locally as the arc-shaped patterns shown in typical fluorescence micrographs collected at different locations (Figure S2b in the Supporting Information). When compared with the surface patterns in Figure 3c,d, no splitting of ellipses was observed (that is, there was no interference from the pinned contact lines). The ellipses maintained their curvatures as the solution front moved toward the chisel lens/Si contact center.

It is noteworthy that these complex structures with unprecedented regularity (Figure 1c,d, Figure 3c,d, and Figure S2b in the Supporting Information) are highly reproducible. The ability to guide a variety of intricate structural formations by evaporation allows for the scale-up of surface patterning over large areas at low cost, and without the need for lithography and external fields.

The present study describes a robust, inexpensive, and one-step method that capitalizes on imposed axially symmetrical geometries to control solvent evaporation and the associated capillary flow of an evaporating microfluid. By simply tailoring the shape of the upper surface, the imposed

geometry directs the formation of a variety of complex, highly regular structures in a precisely controllable manner. As such, this method represents a significant advance in creating regularly organized, complex structures with potential applications in microelectronics, optoelectronics, and biotechnology, among other areas. By rationally designing the upper surface to accommodate different shapes, we envision the possibility of creating an even richer family of surface patterns. Furthermore, there should be no limitation on the solutes that can be applied to form such highly ordered structures. For example, by employing nanocrystals and/or block copolymers,[23] complex multifunctional materials and highly regular devices demonstrating hierarchical order over two or multiple length scales may be created.

Experimental Section

To construct and implement a specific curve-on-flat geometry, both the curved upper surface and the Si substrate were firmly fixed at the top and bottom of sample holders, respectively. An inchworm motor was used to bring the upper surface in contact with the lower stationary Si substrate. Before contact, with only a few hundred micrometers between the surfaces, a solution of MEH-PPV (M_w = 50–300 kg mol^{-1}; American Dye Sources) in toluene (25 μL) was loaded and trapped between the curved surface and the Si by capillary force. The curved surface was finally moved into contact with the Si substrate such that a capillary-held MEH-PPV microfluid formed. Evaporation of the solvent was restricted to the edge of the capillary within the curve-on-flat geometry (Figures 1a and 3a). Experiments were performed at room temperature inside a homemade chamber. Taken together, the evaporation rate of solvent and the associated capillary flow were readily controlled, and the temperature gradient was eliminated.

Received: September 20, 2008
Published online: November 12, 2008

Keywords: microfluids · polymers · self-assembly · surface analysis · surface patterning

[1] T. P. Bigioni, X. M. Lin, T. T. Nguyen, E. I. Corwin, T. A. Witten, H. M. Jaeger, *Nat. Mater.* **2006**, *5*, 265.
[2] C. P. Martin, M. O. Blunt, E. Pauliac-Vaujour, A. Stannard, P. Moriarty, *Phys. Rev. Lett.* **2007**, *99*, 116103.
[3] B. P. Khanal, E. R. Zubarev, *Angew. Chem.* **2007**, *119*, 2245; *Angew. Chem. Int. Ed.* **2007**, *46*, 2195.
[4] E. Rabani, D. R. Reichman, P. L. Geissler, L. E. Brus, *Nature* **2003**, *426*, 271.
[5] Z. Mitov, E. Kumacheva, *Phys. Rev. Lett.* **1998**, *81*, 3427.
[6] R. D. Deegan, O. Bakajin, T. F. Dupont, G. Huber, S. R. Nagel, T. A. Witten, *Nature* **1997**, *389*, 827.
[7] E. Pauliac-Vaujour, A. Stannard, C. P. Martin, M. O. Blunt, I. Notingher, P. J. Moriarty, I. Vancea, U. Thiele, *Phys. Rev. Lett.* **2008**, *100*, 176102.
[8] V. X. Nguyen, K. J. Stebe, *Phys. Rev. Lett.* **2002**, *88*, 164501.
[9] M. Gleiche, L. F. Chi, H. Fuchs, *Nature* **2000**, *403*, 173.
[10] J. Huang, F. Kim, A. R. Tao, S. Connor, P. D. Yang, *Nat. Mater.* **2005**, *4*, 896.
[11] J. Huang, R. Fan, S. Connor, P. D. Yang, *Angew. Chem.* **2007**, *119*, 2466; *Angew. Chem. Int. Ed.* **2007**, *46*, 2414.
[12] S. W. Hong, J. Xu, J. Xia, Z. Q. Lin, F. Qiu, Y. L. Yang, *Chem. Mater.* **2005**, *17*, 6223.
[13] J. Xu, J. Xia, Z. Q. Lin, *Angew. Chem.* **2007**, *119*, 1892; *Angew. Chem. Int. Ed.* **2007**, *46*, 1860.
[14] H. Yabu, M. Shimomura, *Adv. Funct. Mater.* **2005**, *15*, 575.
[15] D. J. Harris, H. Hu, J. C. Conrad, J. A. Lewis, *Phys. Rev. Lett.* **2007**, *98*, 148301.
[16] V. V. Tsukruk, H. Ko, S. Peleshanko, *Phys. Rev. Lett.* **2004**, *92*, 065502.
[17] S. W. Hong, J. Xia, Z. Q. Lin, *Adv. Mater.* **2007**, *19*, 1413.
[18] J. D. Joannopoulos, R. D. Meade, J. N. Winn, *Photonic crystals-modeling the flow of light*, Princeton University Press, Princeton, NJ, **1995**.
[19] H. O. Jacobs, G. M. Whitesides, *Science* **2001**, *291*, 1763.
[20] S. J. Kang, C. Kocabas, T. Ozel, M. Shim, N. Pimparkar, M. A. Alam, S. V. Rotkin, J. A. Rogers, *Nat. Nanotechnol.* **2007**, *2*, 230.
[21] B. J. Schwartz, *Annu. Rev. Phys. Chem.* **2003**, *54*, 141.
[22] D. L. Chen, C. J. Gerdts, R. F. Ismagilov, *J. Am. Chem. Soc.* **2005**, *127*, 9672.
[23] Y. Lin, A. Boker, J. He, K. Sill, H. Xiang, C. Abetz, X. Li, J. Wang, T. Emrick, S. Long, Q. Wang, A. Balazs, T. P. Russell, *Nature* **2005**, *434*, 55.
[24] E. Delamarche, A. Bernard, H. Schmid, B. Michel, H. Biebuyck, *Science* **1997**, *276*, 779.
[25] J. Xu, J. Xia, S. W. Hong, Z. Q. Lin, F. Qiu, Y. L. Yang, *Phys. Rev. Lett.* **2006**, *96*, 066104.
[26] E. Adachi, A. S. Dimitrov, K. Nagayama, *Langmuir* **1995**, *11*, 1057.
[27] S. W. Hong, J. Xia, M. Byun, Q. Zou, Z. Q. Lin, *Macromolecules* **2007**, *40*, 2831.
[28] S. Vyawahare, K. M. Craig, A. Scherer, *Nano Lett.* **2006**, *6*, 271.

